Evaluation of rigid pavement on apron of terminal 3 Soekarno-Hatta International Airport using finite element method

Pamahayu Prawesti[1,*], *Bambang* Suhendro[2], and *Suryo* Hapsoro[3]

[1]Civil and Environmental Engineering Department, Gadjah Mada University, Yogyakarta, Indonesia
[2]Structural Engineering Research Group, Faculty of Engineering, Gadjah Mada University, Yogyakarta, Indonesia
[3]Transport Engineering Research Group, Faculty of Engineering, Gadjah Mada University, Yogyakarta, Indonesia

Abstract. The development of transportation technology is indicated by the appearance of a new aircraft gear configuration, dual trim. The load repetitions of the movement of aircraft with dual-tridem gears, such as B-777-300ER aircraft with MTOW 28 tons, on Terminal 3 Soekarno-Hatta International Airport (SHIA) apron may cause pavement deformation, resulting in long-term fatigue and structural failures. Therefore, the performance of the existing rigid pavements to hold the loads for the next 20 years should be evaluated. Firstly, the equivalent annual departure and coverage of the aircraft in the airport up to 2037 is calculated. Next, the existing rigid pavement structure of the apron in the airport is modeled using a finite element method to calculate thermal stress and fatigue analysis for either the dowel or the slab. Our study result shows that the coverage value for the next 20 years is 86,534 with the maximum deflection of 0.055 mm and the maximum stress of 0.496834 MPa. The calculated thermal stress is 1.55 MPa, resulting in load repetition for the slab 1,241,484 and an infinite load repetition for the dowel.

1 Introduction

1.1 Background

Indonesia's aviation industry has been growing rapidly for the past few years, for both domestic and international travels. It is characterized by the introduction of various types of larger aircraft into the industry. One of the aircraft is dual-tridem gears-based Boeing 777-300ER, operated by PT. Garuda Indonesia since 2013 to serve long-haul international routes from/to Terminal 3 Soekarno-Hatta International Airport (SHIA). The use of heavier aircraft raises concern regarding the capability of the apron's pavement structure on handling the additional loads.

Unfortunately, the current existing airport pavement design guidelines only specify pavement thickness output. The pavement thickness capability gained in restraining the structural response (stress, strain, and deflection) generated by the aircraft load on the landing gear is not covered yet. Therefore, finite element methods are needed to overcome this problem. In addition, the basic theory of pavement loading developed by Westergaard in 1926 can only be applied to single-wheel aircraft and two-layer pavements. This study is conducted to address the limitations of current existing theories that have not accommodated current technology developments.

This study focuses to measure the ability to exist pavements in the apron of Terminal 3 SHIA to resist structural responses due to temperature and load variation. The analysis was performed using a finite element method with the help of Abaqus software version 6.11.

1.2 Objective

The objective of this research is to evaluate of existing rigid pavements on the apron of Terminal 3 Soekarno-Hatta International Airport in support the loads that pass through it during the design life.

2 Theoretical tramework

2.1 Calculation of equivalent annual departure and coverage

1. Determine the annual departures expressed in design aircraft landing gear (R_2).

$$R_2 = Annual\ Departure\ 2017 \times Conversion\ Factor \quad (1)$$

2. Determine the wheel load of design aircraft (W_1) B-777-300ER.

$$W_1 = \%\ load\ on\ main\ gear \times MTW \times \frac{1}{N} \quad (2)$$

where : W_1 = wheel load of design aircraft (kg),

* Corresponding author: pamahayuprawesti@yahoo.co.id

N = number of design aircraft landing gear.

3. Determine the wheel load of the aircraft in question (W_2)

$$W_2 = \%\ \text{load on main gear x MTW x } \frac{1}{N} \quad (3)$$

where :
W_2 = wheel load of the aircraft in question (kg),
N = the number of design aircraft landing gear.

4. Determine equivalent annual departures by the design aircraft (R_1) B-777-300ER.

$$Log\ R_1 = log\ R_2 \text{ x } \left(\frac{W_2}{W_1}\right)^{1/2} \quad (4)$$

where :
R_1 = equivalent annual departures by design aircraft,
R_2 = annual departures expressed in design aircraft landing gear,
W_1 = wheel load of design aircraft (kg),
W_2 = wheel load of the aircraft in question (kg).

5. Coverage

$$Coverage = \frac{R_1 \text{ x } (1+i)}{Pass\ To\ Load\ Repetition} \quad (5)$$

where :
R_1 = equivalent annual departures by design aircraft,
I = growth factor of aircraft movement, B-777-300ER Pass To Load Repetition = 4,05.

2.2 Modulus of rupture of concrete

FAA (1995) explains that flexural strength of concrete can be estimated by compressive strength using this formula:

$$R = 9\sqrt{fc'} \quad (6)$$

where : R = modulus of rupture of concrete (psi),
fc' = compressive strength of concrete (psi).

2.3 Thermal stress

Based on Delatte (2008), the thermal stress due to curling and warping is determined by the ratio between slab length (L) and relative stiffness radius (ℓ). The formula to determine the relative stiffness radius (ℓ) is :

$$\ell = \sqrt[4]{\frac{ED^3}{12\ (1-\upsilon^2)k}} \quad (7)$$

where : ℓ = relative stiffness radius (mm),
E = modulus elasticity of concrete (MPa),
D = pavement thickness (mm),
k = modulus of subgrade reaction (MPa/m),
υ = Poisson's ratio.

The next step is to calculate the stress due to temperature difference using formula :

$$\sigma_{es} = \frac{CE\alpha_t\Delta t}{2(1-\upsilon^2)} \quad (8)$$

where : C = correction factor
E = modulus elasticity of concrete (MPa),
α_t = thermal expansion of concrete (^{0}C),
Δt = temperature difference between top and bottom surface on slab (^{0}C),
υ = Poisson's ratio.

$$W_2 = \%\ \text{load on main gear x MTW x } \frac{1}{N} \quad (9)$$

3 Idealization of finite element modelling for pavement structure

Before the computation is performed on the model, the idealization of modeling is firstly carried out to define some modeling conditions in order to represent the actual pavement conditions. In general, the idealization of modeling includes:

3.1 Global modelling

The global model is made by using solid elements modeled into 12 slabs, with as many as 4 slabs are connected transversely (x-axis-wise) and 3 slabs are connected longitudinally (y-axis-wise). Due to the limited resources available, the connection between slabs in the global model is not made using dowel. In addition, footprints in the global model are footprints on both sides of main landing gear. The footprint is located on the edge of the slab (edge loading). While the other side's footprint is located on the interior of the slab (interior loading). The dimensions of other parts that have been adjusted can be seen in Table 1 and Figure 1.

Table 1. Global modelling part dimension

No	Part	Dimension
1	Slab	5,000mm x 5,000mm
	Thickness	550 mm
2	Elliptical Foot Print	
	Major Axis	598.7 mm
	Minor Axis	374.2 mm
3	Cement Treated Base Course	20,000mm x 15,000mm
	Thickness	150 mm
4	Base Course	20,000mm x 15,000mm
	Thickness	150 mm
5	Subbase	20,000mm x 15,000mm
	Thickness	600 mm
6	Subgrade	20,000mm x 15,000mm
	Thickness	1,500 mm

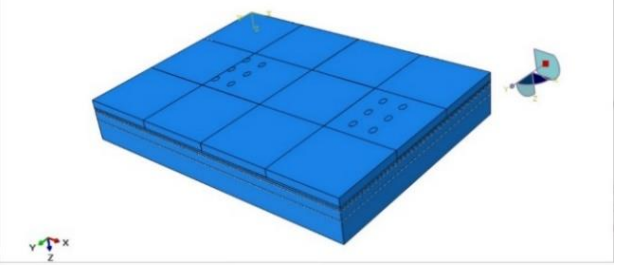

Fig. 1. Global modelling of apron rigid pavement

3.2 Local modelling

The aim of local models is to perform more specific analysis, because it analyzes the stress and deflection on the slab connection, especially the ability of dowel to function properly in transferring loads. They are made using solid elements which use dowels to hold together 2 connected slabs, and between slabs are given a gap of 10 mm. Footprint made in a local model is a footprint on one side of main landing gear. The footprint is located on the joint between slab (edge loading). The dimensions of other parts that have been adjusted can be seen in Table 2 and Figure 2.

Table 2. Local modelling part dimension

No	Part	Dimension
1	Slab	5,000mm x 5,000mm
	Thickness	550 mm
	Spacing	10 mm
2	Elliptical Foot Print	
	Major Axis	598.7 mm
	Minor Axis	374.2 mm
3	Cement Treated Base Course	10,000mm x 5,000mm
	Thickness	150 mm
4	Base Course	10,000mm x 5,000mm
	Thickness	150 mm
5	Subbase	10,000mm x 5,000mm
	Thickness	600 mm
6	Subgrade	10,000mm x 5,000mm
	Thickness	1,500 mm
7	Dowel	
	Diameter	50 mm
	Length	610 mm
	Spacing	460 mm

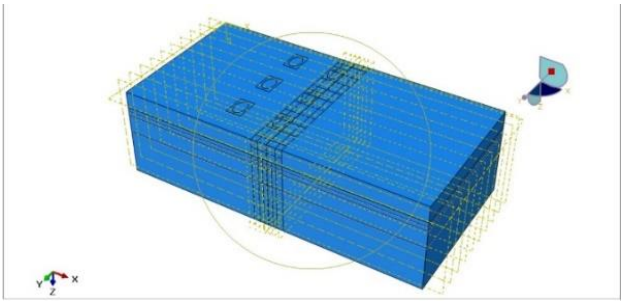

Fig. 2. Local modelling of apron rigid pavement

3.3 Boundary condition

Boundary condition is one of the conditions that must be defined in a finite element modeling. Boundary conditions explain the limitations that a finite element model must have. Because the analysis carried out is a couple-temp displacement which combines two analysis at a time, which are the displacement and temperature analysis, as explained as follows:

a) Displacement (mechanical bouncary condition)

The boundary conditions that must be defined in this model are the hinge (joint) on the bottom surface subgrade and roll on the outer surface of the pavement (the x and y fields). The purpose of the roll boundary condition is to lock the pavement model so that it does not have displacement in the x-axis and y-axis direction, even if the displacement still occurs, the value will not be too large.

b) Temperature

The second boundary condition that must be defined in this model is tmperature on top surface and bottom surface of the concrete. This temperature can have an effect on the structure response that occurs. The temperature value chosen is temperature during the day, because in the daytime, the temperature value are more extreme than at night, as in Table 3 below.

Table 3. Temperature on top and bottom surface of concrete

Surface	Temperature (^{O}C)	
	Day	Night
Top	55	25
Bottom	25	30

4 Result and analysis

4.1 Growth analysis of aircraft movement

The first step in this study is to perform growth analysis of aircraft movement, to predict the movement of aircraft at Soekarno-Hatta International Airport over the next 20 years (up to 2037). The data used in this analysis is the aircraft movement data at SHIA from 2002 to 2017 obtained from PT. Angkasa Pura 2, which can be seen in Table 4. From the data, then the aircraft movement for the next 20 years is extrapolated (Figure 3).

Table 4. Soekarno-Hatta International airport aircraft movement data (Source : PT. Angkasa Pura 2)

Year	Aircraft Movement	i (annual growth)
2002	144,765	-
2003	186,695	28.96%
2004	233,501	25.07%
2005	241,882	3.59%
2006	247,126	2.17%
2007	248,482	0.55%
2008	250,173	0.68%
2009	272,877	9.08%
2010	305,464	11.94%
2011	345,398	13.07%
2012	381,120	10.34%
2013	399,430	4.80%
2014	390,984	-2.11%
2015	386,615	-1.12%
2016	413,781	7.03%
2017	442,214	6.87%

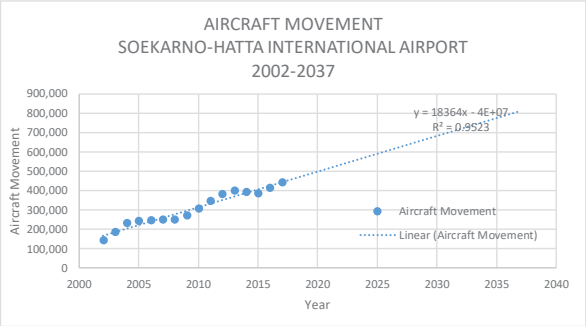

Fig. 3. Forecasting and ekstrapolation of Soekarno-Hatta International airport aircraft movement

4.2 Analysis of equivalent annual departure and coverage

The first stage in calculation of equivalent annual departures is to determine the design aircraft. In this study, the design aircraft used is B-777-300ER aircraft, with the type of main landing gear dual-tridem. The calculation steps are the following :

1. Determine annual departures expressed in design aircraft landing gear (R_2)
   To obtain the value of R2, annual departures of other aircraft in 2017 are converted into annual departures of design aircraft (B-777-300ER).
2. Determine wheel load of design aircraft (W_1) B-777-300ER
   In Boeing 777 Specification document published by Boeing Commercial Airplanes in 2015, the percentage of load for B-777-300ER aircraft on main landing gear is 92.46% and the maximum design taxi weight (MTW) is 352.442 kg, and the number of main landing gear is 12 wheels.
   $$W_1 = 92.46\% \text{ x } 352{,}442 \text{ x } \frac{1}{12} = 27{,}156 \text{ kg}$$
3. Determine wheel load of the aircraft in question (W_2)
   Based on FAA (1995), the percentage of load for mixed aircraft type on the main landing gear is 95%. For example:
   a. Boeing 737-800
      Number of main landing gear : 4
      Landing gear type : dual wheel
      MTW : 7,.333 kg
      W_2 = 95% x 79,333 x ¼ = 18,842 kg
4. Determine equivalent annual departures of design aircraft (R_1) B-777-300ER (Table 5)
5. The calculation of coverage value is done annually for the next 20 years up to 2037 according to the design life (Table 6)

Table 5. Equivalent annual departure (R_1)

No	Aircraft Type	Converted Mixed Annual Departure (R_2)	MTW (kg)	W_2 (kg)	W_1 (kg)	R_1
1	B 727-200	6	95,300	22,634	27,156	6
2	B 737-300	316	63,503	15,082	27,156	73
3	B 737-400	47	68,266	16,214	27,156	20
4	B 737-500	525	61,915	14,705	27,156	101
5	B 737-700	46	70,307	16,698	27,156	21
6	B 737-800	13534	79,333	18,842	27,156	2,763
7	B 737-900	59	79,243	18,821	27,156	30
8	B 737-900ER	3796	85,366	20,275	27,156	1,239
9	B 737-BBJ	2	77,791	18,476	27,156	2
10	B 737 MAX 8	173	82,418	19,575	27,156	80
11	B 747-400	47	397,801	23,620	27,156	37
12	B 747-400 ER	2	414,130	24,589	27,156	2
13	B 747-400 ERF	20	414,130	24,589	27,156	18
14	B 747-400 F	3	397,801	23,620	27,156	3
15	B 757-200	46	116,120	13,790	27,156	16
16	B 767-200	3	143,800	17,077	27,156	3
17	B 767-300BCF	4	187,333	22,246	27,156	4
18	B 767-300ER	68	187,300	22,242	27,156	46
19	B 767-300F	2	187,300	22,242	27,156	2
20	B 777-200	156	287,800	22,785	27,156	103
21	B 777-200ER	86	287,800	22,785	27,156	60
22	B 777-200F	1	352,400	27,899	27,156	1
23	B 777-200LR	3	348,358	27,579	27,156	4
24	B 777-300	515	300,280	23,773	27,156	345
25	B 777-300ER	1743	352,442	27,902	27,156	1,930
26	B 787-800	391	228,384	27,121	27,156	390
27	B 787-900	128	254,692	30,245	27,156	168
28	A 300-200	4	165,900	19,701	27,156	4
29	A 319-132	2	75,900	18,027	27,156	2
30	A 320-200	4422	78,400	18,620	27,156	1,045
31	A 320-214	1060	78,400	18,620	27,156	320
32	A 320-232	309	93,900	22,302	27,156	181
33	A 320-251N	99	93,900	22,302	27,156	65
34	A 321-200	48	93,900	22,302	27,156	34
35	A 321-231	26	93,900	22,302	27,156	20
36	A 330-200	204	242,900	28,845	27,156	241
37	A 330-200F	54	233,900	27,776	27,156	57
38	A 330-243	674	233,900	27,776	27,156	726
39	A 330-300	649	242,900	28,845	27,156	792
40	A 330-302	12	242,000	28,738	27,156	13
41	A 330-343	554	235,000	27,907	27,156	605
42	A 340-300	1	277,400	32,942	27,156	1
43	A 350-900	101	280,900	33,357	27,156	167
44	ANTONOV 12	1	61,000	14,488	27,156	1
45	ATR 42 320	1	37,258	8,849	27,156	1
46	ATR 72-500	1	22,670	5,385	27,156	1
47	ATR 72-600	4	23,000	5,463	27,156	2
48	BAE 146 200	16	43,999	10,450	27,156	6
49	BE20	2	5,711	1,357	27,156	2
50	BEECHCRAFT KING AIR 350	2	6,849	1,627	27,156	2
51	BOMBARDIER CRJ1000	153	41,050	9,750	27,156	21
52	BOMBARDIER CRJ1000 (ER)	153	41,867	9,944	27,156	21
53	CESSNA	1	1,641	780	27,156	1
54	CHALLENGER	1	21,909	5,204	27,156	1
55	EMBRAER 190	59	51,960	12,341	27,156	16
56	EMBREAR LINEAGE 1000	1	54,500	12,944	27,156	1
57	BOMBARDIER GLOBAL EXPRESS (GLEX)	1	45,246	10,746	27,156	1
58	ILYUSHIN IL76/IL 76TD 90VD	2	195,000	11,579	27,156	2
59	MD-82	28	68,266	16,214	27,156	14
TOTAL						**11,833**

Table 6. Coverage

n-th Year	Year	*Equivalent Annual Departures* (R_1)	*Coverage*
0	2017	11,833	2,922
1	2018	12,356	3,051
2	2019	12,755	3,150
3	2020	13,210	3,262
4	2021	13,772	3,401
5	2022	14,334	3,540
6	2023	14,875	3,673
7	2024	15,364	3,794
8	2025	15,776	3,896
9	2026	16,166	3,992
10	2027	16,572	4,092
11	2028	17,040	4,208
12	2029	17,585	4,342
13	2030	18,169	4,487
14	2031	18,693	4,616
15	2032	19,138	4,726
16	2033	19,594	4,839
17	2034	20,077	4,958
18	2035	20,565	5,078
19	2036	21,041	5,196
20	2037	21,509	5,311
TOTAL		**350,424**	**86,534**

4.3 Calculation of contact area

Based on the Boeing 777 specification document issued by Boeing Commercial Airplanes in 2015, the contact area for landing gear of B-777-300ER aircraft was elliptical. The next sttage of this research to calculate the magnitude of major axis and minor axis for elliptical footprint (Figure 4). Based on US Corps of Engineer S-77-1 Report in Rahman (2014), the equations are used:

$$minor\ axis\ (b) = 0.894 \times \sqrt{contact\ area\ (A)} \quad (7)$$

$$major\ axis\ (a) = 1.6 \times minor\ axis\ (b) \quad (8)$$

The magnitude of major axis and minor axis:

$$minor\ axis\ (b) = 0.894\ x\ \sqrt{1{,}752} = 37.42\ cm$$

$$major\ axis\ (a) = 1.6\ x\ 37.42 = 59.87\ cm$$

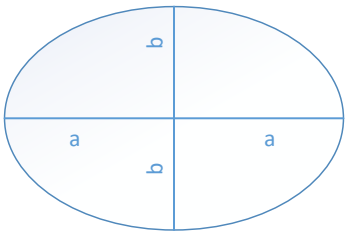

Fig. 4. Elliptical footprint

4.4 Response structure analysis of local and global modelling

The response structure analysis is conducted on loading and joint areas. Previously, the loading area is divided into 3 area. The areas are located on the intersection of critical point for local modelling and global modelling. Area 1 is located on joint between slab of local modelling. Area 2 and area 3 are located on loading area of global modelling. The area can be seen on Figure 5 and Figure 6.

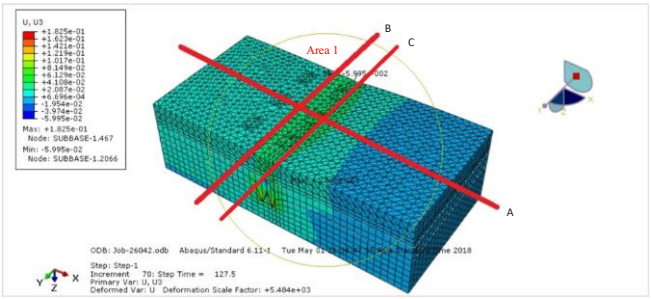

Fig. 5. The intersection of critical point on local modelling (Area 1)

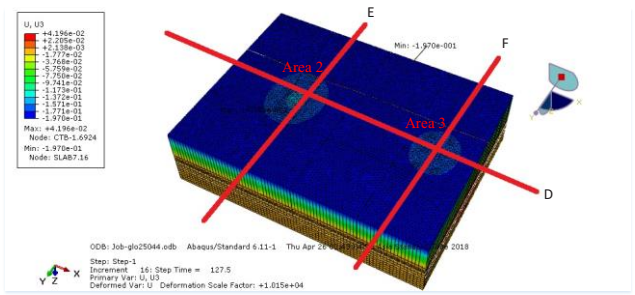

Fig. 6. The intersection of critical point on local modelling (Area 2 and Area 3)

1. Deflection

a. Deflection on loading area

The deflection magnitude of each loading area deflection is illustrated in Table 7. The maximum deflection is illustrated in the form of deflected bowl in Figure 7. The maximum deflection occurs under the load center and on slab joint that is at a distance of 5,000 mm from the slab edge of 0.055 mm.

Table 7. Deflection of loading area

Loading Area	U1 (mm)	U2 (mm)	U3 (mm)
Area 1	0.0194484	0.00312665	-0.0549136
Area 2	0.00524943	0.00413383	-0.0413658
Area 3	0.00285366	0.00280629	-0.0282276

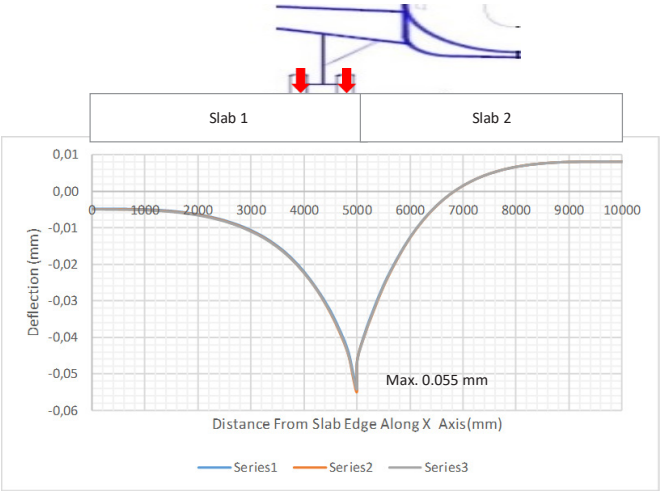

Fig. 7. U3 deflection of intersection point a

b. Deflection on slab joint

The maximum deflection is located at the center of loading area (dowel #5). The maximum deflection for

each dowel can be seen on Table 8 and is illustrated in Figure 8.

Table 8. Deflection on dowel.

Dowel	Maximum Defelection (mm)		
	U1 (mm)	U2 (mm)	U3 (mm)
1	0.000755642	0.000887194	0.0303111
2	0.000208204	0.00118068	0.0363918
3	0.00293899	0.00108362	0.0424083
4	0.00352954	0.000688138	0.0469318
5	0.00386549	0.000261903	**0.0492885**
6	0.00381748	2.49702E-05	0.0483923
7	0.00339568	-0.000023799	0.044841
8	0.00277851	-6.39573E-05	0.0393966
9	0.00180742	-7.05395E-05	0.0324991
10	0.000775807	-5.51546E-05	0.0263213

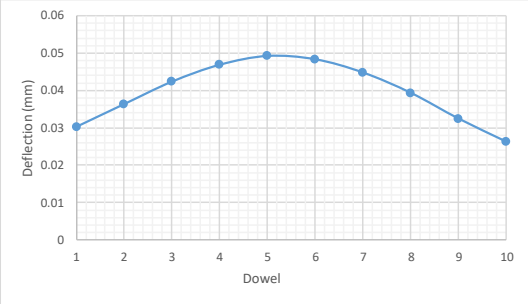

Fig. 8. Deflection on dowel

2. Stress

a. Stress on loading area

The maximum stress in the loading area occurs in the slab and the value is still under the MOR of concrete (Table 9). According to FAA, the MOR value is calculated as follows:

$$R = 9\sqrt{fc'} = 624.53 \text{ psi} = 4.31 \text{ MPa}$$

Where fc′ = compressive strength of concrete (psi) = 4,815.253 psi

b. Stress on slab joint

The maximum stress of dowel occurs in dowel #5, as in Table 10. The value is still below the tensile stress of steel.

$$\text{tensile stress} = 0.83 \text{ x yield stress} = 0.83 \text{ x } 345 = 286{,}35 \text{ MP}a$$

Table 10. Stress on dowel.

Dowel		Maximum Stress (MPa)					
		S11	S22	S33	S12	S13	S23
1	Max	6.08366	3.14488	16.2169	2.77481	0.897628	5.19962
	S/fy	2.12%	1.10%	5.66%	0.97%	0.31%	1.82%
2	Max	15.3565	6.67076	19.1715	3.70483	1.7269	5.23852
	S/fy	5.36%	2.33%	6.70%	1.29%	0.60%	1.83%
3	Max	45.6593	15.9498	22.9732	5.28836	3.93648	4.72629
	S/fy	15.95%	5.57%	8.02%	1.85%	1.37%	1.65%
4	Max	50.9732	17.9397	24.745	5.30461	4.60668	4.68848
	S/fy	17.80%	6.26%	8.64%	1.85%	1.61%	1.64%
5	**Max**	**59.2957**	**20.7584**	**28.934**	**5.43787**	**5.50761**	**5.19841**
	S/fy	**20.71%**	**7.25%**	**10.10%**	**1.90%**	**1.92%**	**1.82%**
6	Max	56.0183	19.7808	28.2801	4.4413	5.03497	4.5661
	S/fy	19.56%	6.91%	9.88%	1.55%	1.76%	1.59%
7	Max	49.8982	17.8671	25.3665	3.60032	4.4474	3.92913
	S/fy	17.43%	6.24%	8.86%	1.26%	1.55%	1.37%
8	Max	39.7314	8.74337	22.5412	2.51951	3.29516	3.72474
	S/fy	13.88%	3.05%	7.87%	0.88%	1.15%	1.30%
9	Max	26.8928	6.01241	18.7475	1.55676	1.97048	3.27086
	S/fy	9.39%	2.10%	6.55%	0.54%	0.69%	1.14%
10	Max	5.73402	3.01778	14.7682	0.708119	0.855936	3.78972
	S/fy	2.00%	1.05%	5.16%	0.25%	0.30%	1.32%

Table 9. Stress on loading area.

Loading Area		S11	S22	S33	S12	S13	S23
Area 1	Max	0.44479	0.242762	0.617681	0.282919	0.371916	0.261559
	S/MOR	10.33%	5.64%	14.34%	6.57%	8.64%	6.07%
	Min	**-0.496834**	-0.0812041	-0.422345	-0.204054	-0.313731	-0.478697
	S/MOR	**-11.54%**	-1.89%	-9.81%	-4.74%	-7.29%	-11.12%
Area 2	Max	0.158272	0.119844	0.0993954	0.0662256	0.027094	0.015048
	S/MOR	3.68%	2.78%	2.31%	1.54%	0.63%	0.35%
	Min	-0.166423	-0.1672	-0.0695927	-0.0521234	-0.0249116	-0.0133992
	S/MOR	-3.86%	-3.88%	-1.62%	-1.21%	-0.58%	-0.31%
Area 3	Max	0.122563	0.0897775	0.0760454	0.0920218	0.0206125	0.0321805
	S/MOR	2.85%	2.08%	1.77%	2.14%	0.48%	0.75%
	Min	-0.166200	-0.166011	-0.049238	-0.0924547	-0.0110901	-0.0322264
	S/MOR	-3.86%	-3.86%	-1.14%	-2.15%	-0.26%	-0.75%

4.4 Thermal stress analysis

The calculation of thermal stress using formula in Delatte (2004). Previously, check the temperature difference that occurs after analysis with Abaqus, as can be seen on Table 11. The thermal stress results are shown in Table 12. The maximum cumulative stress of Abaqus running result and thermal stress, occurs in Area 1 and when the temperature difference of 42.82^{0}C still produces value below the MOR of concrete.

Table 11. Temperature difference between top and bottom surface

Surface	Temperature (^{O}C)		
	Initial Condition	Post Analysis	
		Global Modelling	Local Modelling
Top Surface	55	55	42.0036
Bottom Surface	25	0	-0.811535
Δt (^{O}C)	30	55	42.815135

Table 12. Thermal stress

Δt (°C)	σes (MPa)	Smax (MPa)				σes + Smax (MPa)				MOR (Mpa)		
		Area 1		Area 2	Area 3	Area 1		Area 2	Area 3			
		Slab 1	Slab 2			Slab 1	Slab 2					
30	0.696061	0.553916	0.496834	0.166423	0.1662	1.249977	1.192895	0.862484	0.862261	4.305967	<MOR	OK
35	0.812072	0.553916	0.496834	0.166423	0.1662	1.365988	1.308906	0.978495	0.978272	4.305967	<MOR	OK
40	0.928082	0.553916	0.496834	0.166423	0.1662	1.481998	1.424916	1.094505	1.094282	4.305967	<MOR	OK
42.82	0.993512	0.553916	0.496834	0.166423	0.1662	**1.547428**	1.490346	1.159935	1.159712	4.305967	<MOR	OK
45	1.044092	0.553916	0.496834	0.166423	0.1662	1.598008	1.540926	1.210515	1.210292	4.305967	<MOR	OK
50	1.160102	0.553916	0.496834	0.166423	0.1662	1.714018	1.656936	1.326525	1.326302	4.305967	<MOR	OK
55	1.276113	0.553916	0.496834	0.166423	0.1662	1.830029	1.772947	**1.442536**	1.442313	4.305967	<MOR	OK

4.5 Fatigue analysis

1. Fatigue on Slab

In this research, the S-N curve used is Cornelissen and Reinhardt curves (1984) in CEB (1998) as in Figure 10, with the following formula:

$$\text{Log N} = 8.94 - 7.68\frac{\sigma_{max}}{\text{fctm}} - 0{,}37\frac{\sigma_{min}}{\text{fctm}} \qquad (9)$$

σmax = σes + Smax = 1.547428 MPa

σmin = σes + Smin = 1.0021271 MPa

Thus, the number of load repetition on the slab is 1,241,484 repetitions.

2. Fatigue on Dowel

The maximum stress on dowel is 59.2957 MPa. If the tensile stress for steel is 286.35 MPa, then the maximum

stress ratio is 0.2071. The value of 0.2071 is plotted on the S-N curve taken from Juvinall and Marshek (2012) as shown in Figure 9. From the plotting results, it is known that the number of load repetition is infinite repetition.

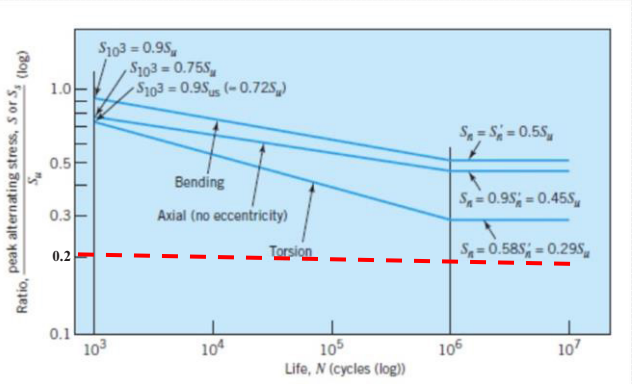

Fig. 9. S-N Curve of steel
(Source : Juvinall and Marshek, 2012)

5 Conclusions and suggestions

5.1 Conclusions

1. The coverage of apron of Soekarno-Hatta Airport Terminal 3 for 20 years is 86,534.
   a. The maximum stress on the concrete slab is 0.496834 MPa for S11. The value is lower than the concrete MOR 4.31 MPa with a stress ratio of 0.1154.
   b. The maximum deflection in vertical direction (U3) is 0.055 mm. The value is below the allowable vertical deflection threshold for apron pavement of 0.5 mm.
2. Structure response analysis is also analyzed in the connection area between slabs (local modeling).
   a. The maximum stress in the connection between slabs (precisely in slab 1) 0.553916 MPa. The value is lower than the concrete MOR of 4.305967 MPa with a stress ratio of 0.1286.
   b. The maximum stress in the dowel is 59.2957 MPa, or 0.2071 from the tensile stress of steel 286.35 MPa.
   c. The maximum deflection vertical direction (U3) of dowel is 0.0492855 mm.
3. The thermal stress of 1.547428 MPa occurs when the temperature difference reaches 42.82^{O}C, the value is lower than the concrete MOR of 4.305967 MPa.
4. Fatigue analysis on slab concrete and dowel.
   a. The number of slab concrete load repetitions is 1,494,376 repetitions.
   b. The number of dowel load repetitions is infinite repetitions.

5.2 Suggestions

1. In order to obtain more accurate results, it is necessary to do finite element method modeling to analyze the effect of load repetition.
2. In order to obtain results that are closer to the actual conditions, thermal stress analysis also can be carried out.
3. To obtain the better results and approach the actual condition, more detailed and depth analysis is needed in the future research.
4. More intensive coordination is needed with PT. Angkasa Pura II in terms of the application of apron pavement data, especially the detailed data about the material properties of pavement as one of the input models, so that the data obtained in accordance with the actual conditions.

References

1. G. Aulia, *Evaluasi Penggunaan Controlled Modulus Column (CMC) Di Bandara Soekarno-Hatta*. Tugas Akhir. Yogyakarta: Jurusan Teknik Sipil dan Lingkungan, Fakultas Teknik, Universitas Gadjah Mada (2015)
2. Boeing Commercial Airplanes, *777-200LR/-300ER/-Freighter Airplane Characteristics for Airport Planning* (2015)
3. M. I. Buchori, *Analisis Perkerasan Kaku Apron Terminal 3 Bandar Udara Internasional Soekarno Hatta Tangerang Banten*. Tugas Akhir. Yogyakarta: Jurusan Teknik Sipil dan Lingkungan, Fakultas Teknik, Universitas Gadjah Mada (2015)
4. J.W. Bull, dan C.H. Woodford, Design of Precast Concrete Pavement Units For Rapid Maintenance of Runways. *Computers and Structures.* **Vol. 64**, No. 1-4, pp. 857-864 (1997)
5. Comite Euro-International Du Beton (CEB), Fatigue of Concrete Structures. State of The Art Report. *Bulletin D'Information No. 188* (1989)
6. N. Delatte, *Concrete Pavement Design, Construction, and Performance.* London: Taylor & Francis (2008)
7. Federal Aviation Administration (FAA), *Airport Pavement Design and Evaluation, Advisory Circular No: 150/5320-6D*. Washington, D.C.: US Government Printing Office (1995)
8. Federal Aviation Administration (FAA), *Airport Pavement Design and Evaluation, Advisory Circular No: 150/5320-6D, Change: 3*. Washington, D.C: US Government Printing Office (2004)
9. Federal Aviation Administration (FAA), *Airport Pavement Design and Evaluation, Advisory Circular No: 150/5320-6E*. Washington, D.C: US Government Printing Office (2009)
10. Federal Aviation Administration (FAA), *Advisory Circular No: AC 150/5300-13A*. Washington, D.C.: US Government Printing Office (2014)
11. Federal Aviation Administration (FAA), *Airport Pavement Design and Evaluation, Advisory Circular No: 150/5320-6F*. Washington, D.C: US Government Printing Office (2016)
12. H.C. Hardiyatmo, *Perancangan Perkerasan Jalan dan Penyelidikan Tanah, Cetakan Pertama*. Yogyakarta : Gadjah Mada University Press (2015)

13. R. Horonjeff, & X. F . McKelvey, *Perencanaan dan Perancangan Bandar Udara (Alih Bahasa).* Jakarta: Penerbit Erlangga (1983)
14. R. Horonjeff, F. X. McKelvvey, W. J. Sproule, & S. B. Young, *Planning and Design of Airports (Fifth Edition).* New york: McGraw-Hill (2010)
15. Y. H. Huang, *Pavement Analysis and Design, Second Edition*. New Jersey : Pearson Education, Inc. (2004)
16. International Civil Aviation Organization (ICAO), *Annex 14* ***Volume I*** *Aerodrome Design and Operations, Seventh Edition, July 2016*. Montreal, Canada : International Civil Aviation Organisation (2016)
17. R.C. Juvinall, & K.M. Mashek, *Fundamentals of Machine Component Design, Fifth Edition.* United States: John Wiley and Sons, Inc. (2008)
18. I. Katili, *Metode Elemen Hingga Untuk Pelat Lentur, Cetakan Pertama*. Jakarta: UI Press (2003)
19. P. B. Kosasih, *Teori dan Aplikasinya : Metode Elemen Hingga.* Yogyakarta: Penerbit ANDI (2012)
20. M.R.K Manesh, M.M.S. Baraki, & A.P. Tavandashti, Examining the Effect of Weight and the Arrangement of Aircrafts' Wheels on Roller-Compacted Concrete (RCC) Pavement Design of Runways Using Finite Element Method. *Current World Environment*. **Vol 10** (Special Issue 1), pp. 574-579 (2015)
21. R. G. Packard, Design of Concrete Airport Pavement. *PCA Engineering Buletin*, hal. 41-47 (1995)
22. T. Rahman, *Evaluasi Kapasitas Dukung dan Nilai PCN Runway Utara Sistem Cakar Ayam Bandar Udara Soekarno-Hatta dengan Permodelan Elemen Hingga (Studi Kasus: Untuk Dilewati oleh Pesawat B777-300ER)*. Tesis. Yogyakarta: Magister Sistem dan Teknik Transportasi, Jurusan Teknik Sipil dan Lingkungan, Fakultas Teknik, Universitas Gadjah Mada (2014)
23. B. Suhendro, *Metode Elemen Hingga dan Aplikasinya.* Yogyakarta : Teknik Sipil – UGM (2000)
24. N. Stromblad, *Modelling of Soil and Structure Interaction Subsea*. Thesis Project. Sweden : Department of Applied Mechanics, Chalmers University of Technology (2014)
25. J.S. Tyau, *Finite Element Modelling Of Reinforced Concrete Using 3-Dimensional Solid Elements With Discrete Rebar*. Master Degree Project. United States of America : Department of Civil and Engineering, Birgham Young University (2009)
26. W.B. Utomo, *Analisis Rigid Pavement dengan Metode Finite Element*. Tesis. Yogyakarta: Magister Sistem dan Teknik Transportasi, Jurusan Teknik Sipil dan Lingkungan, Fakultas Teknik, Universitas Gadjah Mada (2017)
27. E.J. Yoder, dan M.W. Witczak, *Principles of Pavement Design*, *Second Edition.* New York : John Wiley & Sons, Inc. (1975)